Nonlinear Ringdown at the Black Hole Horizon

Neev Khera,[1,*] Ariadna Ribes Metidieri,[2,†] Béatrice Bonga,[2,‡] Xisco Jiménez Forteza,[3,4,5,6,§] Badri Krishnan,[2,3,4,‖] Eric Poisson,[1,¶] Daniel Pook-Kolb,[2,3,4,**] Erik Schnetter,[7,8,9] and Huan Yang[7,1,††]

[1]*University of Guelph, Guelph, Ontario N1G 2W1, Canada*
[2]*Institute for Mathematics, Astrophysics and Particle Physics, Radboud University, Heyendaalseweg 135, 6525 AJ Nijmegen, The Netherlands*
[3]*Albert-Einstein-Institut, Max-Planck-Institut für Gravitationsphysik, Callinstraße 38, 30167 Hannover, Germany*
[4]*Leibniz Universität Hannover, 30167 Hannover, Germany*
[5]*Nikhef, Science Park 105, 1098 XG Amsterdam, The Netherlands*
[6]*Institute for Gravitational and Subatomic Physics (GRASP), Utrecht University, Princetonplein 1, 3584 CC Utrecht, The Netherlands*
[7]*Perimeter Institute for Theoretical Physics, Ontario N2L 2Y5, Canada*
[8]*Department of Physics and Astronomy, University of Waterloo, Ontario, Canada*
[9]*Center for Computation & Technology, Louisiana State University, Baton Rouge, Louisiana, USA*

(Received 14 July 2023; accepted 30 October 2023; published 6 December 2023)

The gravitational waves emitted by a perturbed black hole ringing down are well described by damped sinusoids, whose frequencies are those of quasinormal modes. Typically, first-order black hole perturbation theory is used to calculate these frequencies. Recently, it was shown that second-order effects are necessary in binary black hole merger simulations to model the gravitational-wave signal observed by a distant observer. Here, we show that the horizon of a newly formed black hole after the head-on collision of two black holes also shows evidence of nonlinear modes. Specifically, we identify one quadratic mode for the $l = 2$ shear data, and two quadratic ones for the $l = 4$, 6 data in simulations with varying mass ratio and boost parameter. The quadratic mode amplitudes display a quadratic relationship with the amplitudes of the linear modes that generate them.

DOI: 10.1103/PhysRevLett.131.231401

Introduction.—Gravitational wave observations are increasing rapidly and with them the science we can extract from these observations. Some examples are the statistical inference of the mass distribution of stellar mass black holes in our universe (see, e.g., [1–4]), lessons on the formation of heavy elements in the merger of binary neutron stars [5], and tests of strong-field gravity and black holes (see, e.g., [6–12]). For the latter, black hole spectroscopy is a valuable tool [6,13–18]. This method relies on the fact that after the merger of two black holes, the newly formed object settles down to a new stationary black hole by emitting gravitational waves with a discrete set of complex frequencies called quasinormal modes (QNMs). These QNMs depend only on the two parameters describing black holes: their mass M and spin J. If more than one QNM can be observed, one can test for consistency of these modes (as has been done in [19,20]). Black hole spectroscopy requires the observation of multiple QNMs, which in turn depends not only on the strength of the gravitational wave signal but also on our ability to model these modes accurately. Linear perturbation theory on a Kerr spacetime can be used to calculate the linear frequencies of the QNMs [21–25], analyze gravitational wave observations [26,27], and make forecasts for the detectability of QNMs [7,17,28]. Studies of numerical waveforms have shown the importance of various effects of the linear modes, including higher overtones, mirror modes, mode mixing, and the influence of the Bondi-Metzner-Sachs frames [29–32].

However, nonlinearities are naturally expected in the ringdown stage [33–38]. In particular, it has been shown that modes with a frequency expected from perturbation theory at quadratic order fit the ringdown phase better than higher overtones in the linear theory [19,20,39,40] (see also pioneering work in [41]). This is an important result both conceptually, as general relativity is a nonlinear theory after all, and practically as these quadratic QNMs may be detectable in observations and thereby improve our strong-field tests of general relativity and black holes.

The source emitting gravitational radiation—in the case of QNMs, the time-dependent merger object that settles down to a Kerr black hole—emits waves that go out to infinity and fall into the horizon. The waves at infinity are the ones we observe and interpret as QNMs, but numerical simulations have indicated that the shear modes at the horizon are also accurately described by a superposition of modes with frequencies matching those of the signal at infinity [42]. Given that the horizon is in the strong field regime, one would naturally expect that the signal at the horizon should also show evidence of nonlinearities. In

 © 2023 American Physical Society

TABLE I. Mass ratio μ and momentum parameter P of nine simulations of the head-on collision of two Schwarzschild black holes.

Simulation	$S1$	$S2$	$S3$	$S4$	$S5$	$S6$	$S7$	$S8$	$S9$
$\mu = m_1/m_2$	1	1.6	2	3	1	1	1	1	1
P	0	0	0	0	0.90	1.20	1.52	1.80	2.10

particular, one would expect the shear modes to be better fitted by a model that takes the next-to-leading order QNM frequencies into account than a model based on frequencies derived solely from linear perturbation theory. We investigated this for simulations of head-on collisions of two black holes. We find evidence for the presence of a single quadratic tone in the shear mode $l = 2$, and of two quadratic tones in the shear mode $l = 4$ and 6.

Hence, nonlinearities are present both at infinity and near the horizon. This invalidates the idea that nonlinearities may be hidden behind the horizon or are even absent [29,39,43–46].

Setup.—We study the head-on collision of nonspinning black holes with different boost parameters and mass ratios, as summarized in Table I. In particular, we investigate two sets of simulations. The first set ($S1$–$S4$) describes black holes initially at rest with Brill-Lindquist's bare masses m_1 and m_2 [47]. The second set ($S5 - S9$) are equal-mass black holes with Bowen-York initial data [48], in which both black holes have an equal and opposite Bowen-York momentum parameter of magnitude P expressed in units of $M_\circ = m_1 + m_2$, the total bare mass [49].

The boosted simulations have larger linear amplitudes than the unboosted ones, typically by a factor of 10. Consequently, the quadratic amplitudes are also larger in these boosted simulations and it is easier to confidently establish their presence for larger l modes.

We track the evolution of the outermost marginally outer trapped surface (MOTS), which traces out a $2+1$-dimensional world-tube $\mathcal{H}$ and is the dynamical black hole horizon of the newly formed black hole at $t = 0$ ($t = 1.06M$) for the boosted (unboosted) simulations. Initially, this surface is highly distorted and dynamic, but it quickly settles down to a nearly spherical MOTS as the black hole approaches a Schwarzschild solution. We define the onset of the ringdown as the time during which the change in the area of the MOTS becomes oscillatory and below 1%. In practice, we take $t_{\rm rd} = 8.2M$, where M is the mass of the remnant, such that all simulations have reached this ringdown regime. This makes it easier to compare the simulations. Having access to the evolution of the horizon area allows us to avoid the contamination in our data from the merger phase, a common issue in this type of analysis, discussed in depth in [19,20]. We follow the horizon evolution until $t_{\rm f} \approx 40M$ for the unboosted simulations and $t_{\rm f} \approx 32M$ for the boosted ones.

The shear of the outward null normal ℓ to the MOTS is a measure of the gravitational waves going into the horizon [43,50], but also a geometric quantity measuring the deformation of the horizon surface. In the following, we focus uniquely on the shear, although a complementary study using the mass multipole moments shows qualitatively similar results. We fix a unique ℓ via $\ell^a \nabla_a t = 1$, where ∇_a is the spacetime covariant derivative and t is the coordinate time of the simulation. The shear σ of ℓ is then calculated similarly to [42], but we also multiply by the remnant mass to make it dimensionless.

During the ringdown, we can decompose σ at the horizon as a sum of damped sinusoids [42], namely,

$$\sigma(t,\theta,\varphi) = \sum_{l\geq s,m,n,\pm} \mathcal{A}_{lmn} e^{-i\omega^{\pm}_{lmn}(t-t_{\rm rd})+i\phi_{lmn}} {}_2Y_{lm}(\theta,\varphi) \equiv \sum_{l\geq s,m} \sigma_{lm2} Y_{lm}(\theta,\varphi) \tag{1}$$

where the (l,m) indices describe the angular decomposition of the modes (with $m = -l,\ldots,l$), $\mathcal{A}_{lmn}$ are the constant (dimensionless) amplitudes, ϕ_{lmn} the phases, ${}_2Y_{lm}$ the spin-weighted spherical harmonics with spin-weight $s = 2$ and $\omega^{\pm}_{lmn}$ the complex frequencies corresponding to the corotating $\mathrm{Re}[\omega^{+}_{lmn}] > 0$ and counter-rotating $\mathrm{Re}[\omega^{-}_{lmn}] < 0$ modes. The $n = 0, 1, 2, \ldots$ denote the n-tone excitation of a given (l,m) mode, with $n = 0$ being the fundamental tone and $n \geq 1$ correspond to overtones. Because of the rotational symmetry of the head-on collision, the shear is fully described by the $m = 0$ modes and $\omega^{+}_{lmn} = |\omega^{-}_{lmn}|$, so we work with $\omega_{ln} = \omega^{+}_{l0n} = -\omega^{-}_{l0n}$. Hence, we set $m = 0$ and drop the m subindex in both the shear modes $\sigma_{l0} = \sigma_l$ and the complex frequencies. Additionally, all odd l modes vanish for the boosted simulations since the mass ratio is one. Further, by the symmetries of the problem, σ_l is a real-valued function, so the positive and negative frequencies combine to provide a manifestly real expansion of the shear modes

$$\sigma_l = \sum_{n=0}^{n_{\max}} \Big\{ C_{ln} e^{-\mathrm{Im}[\omega_{ln}](t-t_{\rm rd})} \cos(\mathrm{Re}[\omega_{ln}](t-t_{\rm rd})) + S_{ln} e^{-\mathrm{Im}[\omega_{ln}](t-t_{\rm rd})} \sin(\mathrm{Re}[\omega_{ln}](t-t_{\rm rd})) \Big\}. \tag{2}$$

Here C_{ln} and S_{ln} are real amplitudes with $2\mathcal{A}_{ln} = \sqrt{C^2_{ln} + S^2_{ln}}$, and $\tan\phi_{ln} = -S_{ln}/C_{ln}$ [42].

Using black hole perturbation theory, one can calculate the values of the QNM frequencies rather straightforwardly to linear order in the metric perturbations (see the efficient open software routine in [51]). The next order in perturbation theory is rather involved (see Refs. [52–57]) but for each pair of linear QNM frequencies ω_{ln} and $\omega_{l'n'}$, we expect a corresponding quadratic QNM frequency

TABLE II. The slope in Eq. (3) for different quadratic modes present for different l modes. For the boosted simulations, we detect the presence of the quadratic tones when using models with the fundamental mode, one overtone and one quadratic mode ($l = 2$) or the fundamental tone and two quadratic modes ($l = 4$ and $l = 6$), while for the unboosted $l = 2$ shear mode we need to include at least one additional linear overtone. We marked with an asterisk the results for the shear mode $l = 6$ since the models with either the quadratic frequencies $\omega_{20\times60}$ or $\omega_{40\times40}$ are possible, as explained in the Supplementary Material. We present both possibilities here, the second one, including the tones $\omega_{20\times40}$ and $\omega_{40\times40}$, is differentiated in bold.

Mode	$\omega_{ln\times l'n'}$	Boosted (α)	Unboosted (α)
$l = 2$	$\omega_{20\times20}$	$1.51^{+0.15}_{-0.04}$	$6.21^{+0.15}_{-1.15}$
$l = 4$	$\omega_{20\times20}$	$0.73^{+0.06}_{-0.33}$	
	$\omega_{20\times40}$	$2.6^{+0.26}_{-0.26}$	
$l = 6*$	$\omega_{20\times40}$	$1.78^{0.53}_{-0.74}$	
	$\omega_{20\times60}$	$2.52^{+1.29}_{-0.59}$	
	$\boldsymbol{\omega_{20\times40}}$	$\mathbf{1.78^{0.44}_{-0.65}}$	
	$\boldsymbol{\omega_{40\times40}}$	$\mathbf{2.82^{+1.5}_{-0.62}}$	

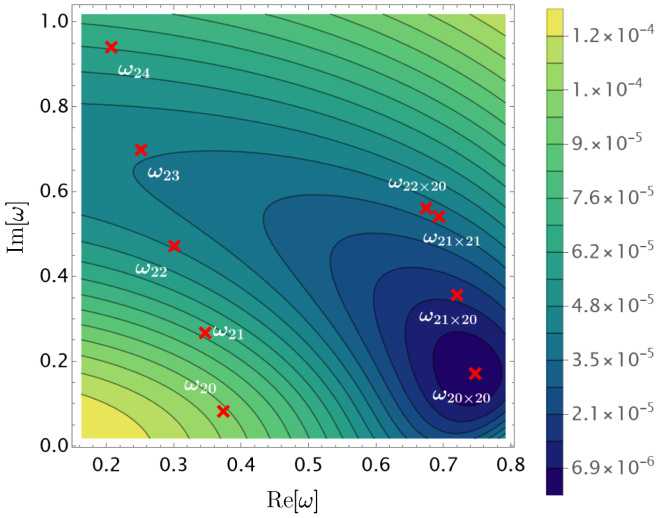

FIG. 1. Mismatch between the $l = 2$ data ($t \in [t_{\rm rd}, t_f]$) of the boosted simulation $S7$ starting at time $t_{\rm rd}$ and a model for σ_2 with three tones, in which two frequencies are fixed to the general relativity predictions ω_{20} and ω_{21}, and the third one is varied.

$\omega_{ln\times l'n'} = \omega_{ln} + \omega_{l'n'}$. We find evidence of quadratic frequencies in the shear modes $l = 2$, 4, and 6, which we show in Table II. Our analysis is inconclusive for the $l = 3$ mode in the unboosted simulations and the $l = 8$ in the boosted ones due to the signal's weak amplitude.

Here, we only present the detailed analysis for the $l = 2$ shear modes of the boosted simulation $S7$ with a spatial discretization, $\Delta x = M_\circ/\text{res}$, where $M_\circ$ is the total bare mass and "res" refers to the resolution of the grid spacing. The results presented here for $S7$ use res = 120. We also briefly discuss the results for the unboosted simulation $S2$ with res = 312. The details for the remaining simulations in Table I are not discussed explicitly, since they are completely analogous to the ones presented here. The results for higher l modes can be found in the Supplemental Material [58].

Mismatch and stability.—When fitting the data, several combinations of linear and quadratic tones are possible. To minimize the risk of overfitting as discussed in [19,20,59], we consider a model with the lowest possible number of tones for which the quadratic mode is resolved [60]. For the boosted simulations, a model with three tones suffices [$n_{\rm max} = 2$ in Eq. (2)], while for the unboosted ones, we need a model with at least four tones ($n_{\rm max} = 3$). We analyze the boosted and unboosted simulations independently, so we only compare models with the same number of modes (and thus the same number of free parameters). Using that the QNM model (2) is linear in $C_{\ell n}$ and $S_{\ell n}$, we use a linear least square fitting algorithm to minimize the L^2 norm of the residual. A nonlinear fitting algorithm, such as the one used in [42], yields completely analogous results.

We first explore which quadratic modes could be present in our ringdown dataset $t \in [t_{\rm rd}, t_{\rm f}]$ by scanning over the complex frequency of the last overtone in the model (2). We compute the mismatch (see Ref. [42] for its definition) for each possible frequency of the last overtone. The model with the smallest mismatch is considered the best model. Figure 1 shows that the quadratic frequencies $\omega_{20\times20}$ and $\omega_{21\times20}$ are favored over the linear overtone ω_{22}. The unboosted simulations show the same trend.

We then assess the presence of these quadratic tones by ensuring that they persist when narrowing our dataset. Specifically, we compute the mismatch for the different models while varying the starting time of the dataset to later times $t_0 \in [t_{\rm rd}, 25M]$. Figure 2(a) shows that the models containing the quadratic frequencies $\omega_{20\times20}$ and $\omega_{21\times20}$ have lower mismatch at earlier times, when these modes are expected to be resolvable. In Fig. 2(b), we track the stability of the fit in this process, i.e., the evolution of the mode's amplitudes with the starting time t_0. The model including the quadratic frequency $\omega_{20\times20}$ is the most stable, with a maximum relative variation at early times $t \in [t_{\rm rd}, 15M]$ of $\sim$2% for the fundamental tone's amplitude and $\sim$30% for the amplitudes of the first overtone and the quadratic tone. As already noticed in [42], the model with two linear overtones has amplitudes varying over several orders of magnitude and is therefore unstable: the maximum relative variation of the fundamental tone's amplitude is $\sim$10% while for the first and second overtones, it is $\sim$60% and $\sim$80%, respectively.

We finally consider the model (2) not only with free amplitudes and phases but also with the frequency of the

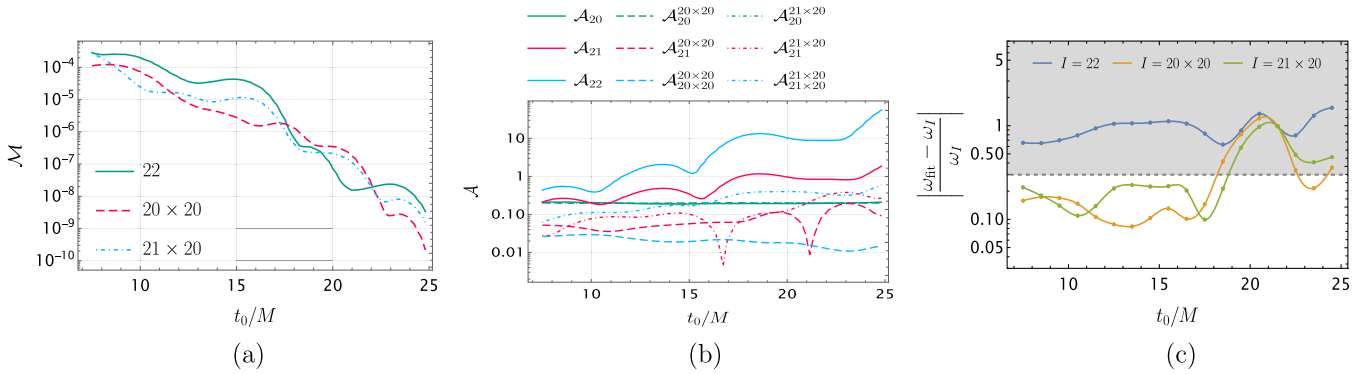

FIG. 2. Mismatch, amplitudes, and best-fitted frequency between the $l = 2$ data of the boosted simulation $S7$ and a model for σ_2 with three tones as a function of the starting time $t_0 \in [t_{\rm rd}, 25M]$ (a) Mismatch of the three models with the third tone's frequency ω_{22}, $\omega_{20\times20}$ or $\omega_{21\times20}$; (b) Amplitudes of the three QNMs for the linear (no superindex) and quadratic models; (c) Relative variation of the optimal frequency with respect to ω_{22}, $\omega_{20\times20}$ and $\omega_{21\times20}$.

last overtone free. We then implement an algorithm of mismatch minimization to find the frequency for which the fit over the dataset $t \in [t_0, t_{\rm f}]$ is optimal. In other words, we effectively track the frequency in Fig. 1 for which the mismatch is minimal as we vary the starting time. Figure 2(c) shows the relative variation of the optimal frequency $\delta\omega = (\omega_{\rm fit} - \omega_{\rm known})/\omega_{\rm known}$ with respect to known possible frequencies (with $\omega_{\rm known} = \omega_{ln\times l'n'}, \omega_{ln}$). The advantage of this procedure is that it sets an absolute lower bound to the mismatch by finding the optimal numerical frequency, and consequently, it enables us to discard possible tones in our model. In fact, Fig. 2(c) shows that a linear model is not favored, not even when the quadratic modes have already decayed since the deviation of the linear overtone with respect to the optimal frequency remains above 50% at all starting times. Further, Fig. 2(c) also shows that both quadratic frequencies $\omega_{20\times20}$ and $\omega_{21\times20}$ have a minimum deviation with respect to the optimal frequency of about 7% and only surpass the 30% deviation once the $l = 2$ shear mode can be accurately described by the fundamental tone (around $t = 20M$). This deviation is consistent with the criteria used in Fig. 1 in [39], and therefore the quadratic frequencies $\omega_{20\times20}$ and $\omega_{21\times20}$ are good candidates to be in our model. The amplitude relation detailed in the next section confirms the presence of the quadratic tone $\omega_{20\times20}$.

Amplitude relations.—The amplitudes of the quadratic modes are related to the ones of the linear modes through

$$\mathcal{A}_{ln\times l'n'} = \alpha \mathcal{A}_{ln}\mathcal{A}_{l'n'}, \tag{3}$$

where α is the slope of the line passing through the origin. If a quadratic mode is present in our data, then we should be able to confirm its presence by fitting Eq. (3) across different simulations. Otherwise, the presence of the quadratic mode could be a consequence of overfitting or an artifact of the mode mixing. We analyze the nonboosted ($S1$–$S4$) and boosted ($S5$–$S9$) simulations independently. In this part of the analysis, we used lower resolution simulations, as these were accurate enough (in particular, we used a resolution of 120 for the boosted and at least 90 for the unboosted simulations).

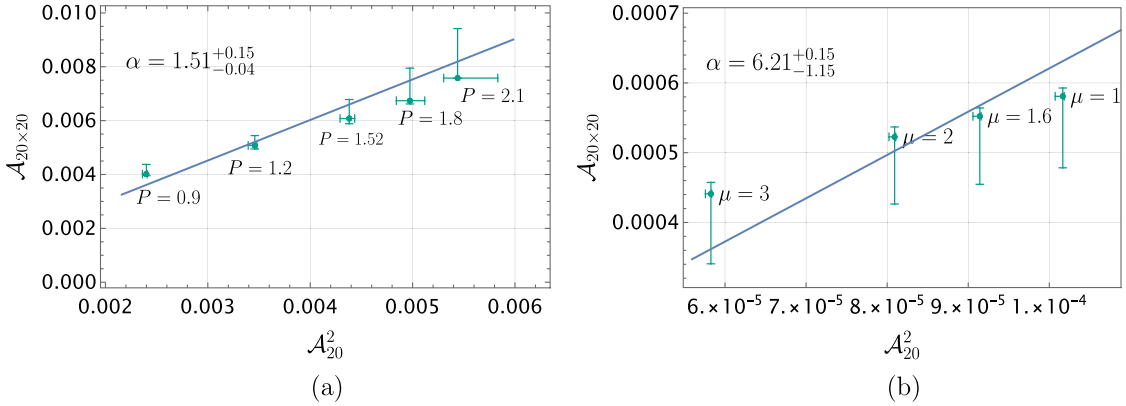

FIG. 3. Amplitude relation for the quadratic tone $\omega_{20\times20}$ in the shear mode $l = 2$ when considering both the boosted and unboosted simulations. In both cases the dataset initial time t_0 is fixed to $t_0 = 15M$. (a) Boosted simulations with constant mass ratio $\mu = 1$; (b) Unboosted simulations with different mass ratios (and momentum parameter $P = 0$).

Figure 3 shows the amplitude relation for the $l = 2$ shear mode. In both sets of simulations, such a relation is found at late times $t_0 \geq 15M$ within the uncertainty bars [61]. At earlier times, the presence of higher overtones blurs this relationship. This analysis confirms the presence of the quadratic frequency $\omega_{20\times20}$ in the $l = 2$ shear mode. The slope in Eq. (3) is reported in Table II.

Given that the remnant black hole in both sets of simulations is Schwarzschild, one might have expected the slopes in the two sets of simulations to be comparable. We see instead that the slopes in the two sets of simulations are inconsistent. This could be because the error bars do not capture systematic modeling errors, for instance, due to the finite separation of the holes in our initial data, inherent to this type of numerical simulations. Additionally, initial conditions are more important than one may naively think. In [38], the authors showed that the slope of the amplitude relation when solving the second-order Teukolsky equation is three times smaller than the slope obtained from the nonlinear numerical simulations in [39] and [40]. A detailed study of such systematic errors, including spin effects, will be presented elsewhere.

In Table II, we collect the slopes for the quadratic relation Eq. (3) of the quadratic tones that we found for the $l = 2$, 4, and 6 shear modes. For the $l = 2$ shear mode, we only include the quadratic tone $\omega_{20\times20}$, since the amplitude relation for the quadratic frequency $\omega_{21\times20}$ is not satisfied for the set of boosted simulations within the uncertainty bars (see Fig. 7 in the Supplemental Material), and therefore we conclude this mode is not present in the $l = 2$ shear mode given our resolution. For the $l = 4$ shear mode we find that a model with the fundamental tone and two quadratic tones, the $\omega_{20\times20}$ and $\omega_{20\times40}$, is the most favored. Both quadratic tones satisfy the amplitude relation over several boosted simulations, and their slopes have been therefore included in Table II. Finally, for the $l = 6$ shear mode, we also find that a model with the fundamental mode and two quadratic ones is the most suitable to fit the shear data. In this case, models including the quadratic frequencies $\omega_{20\times40}$ and $\omega_{20\times60}$ or $\omega_{20\times40}$ and $\omega_{40\times40}$ are both possible, and the small difference in the fit residuals between the two prevents us from opting for one or the other. The figures and the full discussion for the $l = 4$ and 6 shear modes can be found in the Supplemental Material. We would like to highlight that we find the same combination of relevant modes as Cheung *et al.* [39] for the $l = 4$ mode, which provides us with new and novel evidence of arising correlations between the horizon dynamics and the gravitational wave radiation.

Conclusion.—While black hole horizon simulations have existed for a while and one naturally expects the nonlinear nature of general relativity to be important in this regime, this is the first demonstration of nonlinear effects at the horizon. In particular, we have shown that the $l = 2$, 4, 6 shear modes at the horizon—a strong field regime—soon after a head-on collision of two black holes are better fitted with a model that includes next-to-leading order effects in perturbation theory than a purely linear model. These quadratic modes are in agreement with those found by [39] at infinity. Finding the presence of quadratic modes was subtle, it required (1) high-accuracy numerical data, and/or (2) a signal with large linear amplitudes so that the corresponding quadratic amplitudes are also large (as is the case for a boosted signal).

The excitement of observing electromagnetic signals often stems from their origin in "interesting" objects, which allows us to gain insights into the emitter's properties. While the initial detection of gravitational waves was inherently thrilling, gravitational waves increasingly become a tool to investigate the sources emitting them. Black holes are ideal sources to investigate with gravitational waves given their blackness. However, to maximize our understanding of black holes and their horizons, it is crucial to establish a clear connection between the gravitational wave observed at infinity and the horizon geometry. This work is a small step in that direction by showing that just as the wave at infinity, also the horizon geometry of black holes requires nonlinear effects to accurately describe it. It is worth noting the intriguing possibility of a connection with the Kerr/CFT correspondence, as suggested in [62].

The authors are grateful to Mark Ho-Yeuk Cheung, Thomas Helfer, and Emanuele Berti for useful discussions on the GRChombo head-on data, and to Gregorio Carullo for his useful comments on the manuscript. N. K., E. P., and H. Y. are supported by the Natural Science and Engineering Council of Canada. E. S. and H. Y. are supported by Perimeter Institute for Theoretical Physics. Research at Perimeter Institute is supported in part by the Government of Canada through the Department of Innovation, Science and Economic Development Canada and by the Province of Ontario through the Ministry of Colleges and Universities.

[*] nkhera@uoguelph.ca
[†] ariadna.ribesmetidieri@ru.nl
[‡] bbonga@science.ru.nl
[§] frjifo@aei.mpg.de
[‖] badri.krishnan@ru.nl
[¶] epoisson@uoguelph.ca
[**] daniel.pook.kolb@aei.mpg.de
[††] hyang@perimeterinstitute.ca

[1] B. P. Abbott *et al.* (LIGO Scientific and Virgo Collaborations), Astrophys. J. Lett. **818**, L22 (2016).
[2] R. Abbott *et al.* (KAGRA, VIRGO, and LIGO Scientific Collaborations), Phys. Rev. X **13**, 011048 (2023).
[3] S. Libanore, M. Liguori, and A. Raccanelli, J. Cosmol. Astropart. Phys. 08 (2023) 055.
[4] A. H. Nitz, S. Kumar, Y.-F. Wang, S. Kastha, S. Wu, M. Schäfer, R. Dhurkunde, and C. D. Capano, Astrophys. J. **946**, 59 (2023).

[5] R. Diehl, A. J. Korn, B. Leibundgut, M. Lugaro, and A. Wallner, Prog. Part. Nucl. Phys. **127**, 103983 (2022).
[6] E. Berti, K. Yagi, H. Yang, and N. Yunes, Gen. Relativ. Gravit. **50**, 49 (2018).
[7] R. Abbott *et al.* (LIGO Scientific, VIRGO, and KAGRA Collaborations), arXiv:2112.06861.
[8] B. P. Abbott *et al.* (LIGO Scientific and Virgo Collaborations), Phys. Rev. D **100**, 104036 (2019).
[9] S. Kastha, C. D. Capano, J. Westerweck, M. Cabero, B. Krishnan, and A. B. Nielsen, Phys. Rev. D **105**, 064042 (2022).
[10] M. Isi, M. Giesler, W. M. Farr, M. A. Scheel, and S. A. Teukolsky, Phys. Rev. Lett. **123**, 111102 (2019).
[11] M. Isi, W. M. Farr, M. Giesler, M. A. Scheel, and S. A. Teukolsky, Phys. Rev. Lett. **127**, 011103 (2021).
[12] X. J. Forteza, S. Bhagwat, S. Kumar, and P. Pani, Phys. Rev. Lett. **130**, 021001 (2023).
[13] E. Berti, A. Sesana, E. Barausse, V. Cardoso, and K. Belczynski, Phys. Rev. Lett. **117**, 101102 (2016).
[14] H. Yang, K. Yagi, J. Blackman, L. Lehner, V. Paschalidis, F. Pretorius, and N. Yunes, Phys. Rev. Lett. **118**, 161101 (2017).
[15] S. Ma, L. Sun, and Y. Chen, Phys. Rev. Lett. **130**, 141401 (2023).
[16] S. L. Detweiler, Astrophys. J. **239**, 292 (1980).
[17] O. Dreyer, B. J. Kelly, B. Krishnan, L. S. Finn, D. Garrison, and R. Lopez-Aleman, Classical Quantum Gravity **21**, 787 (2004).
[18] E. Berti, V. Cardoso, and C. M. Will, AIP Conf. Proc. **873**, 82 (2006).
[19] P. J. Nee, S. H. Völkel, and H. P. Pfeiffer, Phys. Rev. D **108**, 044032 (2023).
[20] V. Baibhav, M. H.-Y. Cheung, E. Berti, V. Cardoso, G. Carullo, R. Cotesta, W. Del Pozzo, and F. Duque, arXiv:2302.03050.
[21] S. A. Teukolsky, Astrophys. J. **185**, 635 (1973).
[22] E. W. Leaver, Proc. R. Soc. A **402**, 285 (1985).
[23] E. Berti, V. Cardoso, and A. O. Starinets, Classical Quantum Gravity **26**, 163001 (2009).
[24] H. Yang, D. A. Nichols, F. Zhang, A. Zimmerman, Z. Zhang, and Y. Chen, Phys. Rev. D **86**, 104006 (2012).
[25] H. Yang, A. Zimmerman, A. Zenginoğlu, F. Zhang, E. Berti, and Y. Chen, Phys. Rev. D **88**, 044047 (2013).
[26] S. Chandrasekhar and S. L. Detweiler, Proc. R. Soc. A **344**, 441 (1975).
[27] B. P. Abbott *et al.* (LIGO Scientific and Virgo Collaborations), Phys. Rev. Lett. **116**, 221101 (2016); **121**, 129902(E) (2018).
[28] C. D. Capano, M. Cabero, J. Westerweck, J. Abedi, S. Kastha, A. H. Nitz, Y.-F. Wang, A. B. Nielsen, and B. Krishnan, arXiv:2105.05238.
[29] M. Giesler, M. Isi, M. A. Scheel, and S. A. Teukolsky, Phys. Rev. X **9**, 041060 (2019).
[30] A. Dhani, Phys. Rev. D **103**, 104048 (2021).
[31] X. Li, L. Sun, R. K. L. Lo, E. Payne, and Y. Chen, Phys. Rev. D **105**, 024016 (2022).
[32] L. M. Zertuche, K. Mitman, N. Khera, L. C. Stein, M. Boyle, N. Deppe, F. Hébert, D. A. Iozzo, L. E. Kidder, J. Moxon *et al.*, Phys. Rev. D **105**, 104015 (2022).
[33] M. Campanelli and C. O. Lousto, Phys. Rev. D **59**, 124022 (1999).
[34] H. Yang, A. Zimmerman, and L. Lehner, Phys. Rev. Lett. **114**, 081101 (2015).
[35] H. Yang, F. Zhang, S. R. Green, and L. Lehner, Phys. Rev. D **91**, 084007 (2015).
[36] J. L. Ripley, N. Loutrel, E. Giorgi, and F. Pretorius, Phys. Rev. D **103**, 104018 (2021).
[37] L. Sberna, P. Bosch, W. E. East, S. R. Green, and L. Lehner, Phys. Rev. D **105**, 064046 (2022).
[38] J. Redondo-Yuste and L. Lehner, J. High Energy Phys. 02 (2023) 240.
[39] M. H.-Y. Cheung *et al.*, Phys. Rev. Lett. **130**, 081401 (2023).
[40] K. Mitman *et al.*, Phys. Rev. Lett. **130**, 081402 (2023).
[41] L. London, D. Shoemaker, and J. Healy, Phys. Rev. D **90**, 124032 (2014); **94**, 069902(E) (2016).
[42] P. Mourier, X. Jiménez Forteza, D. Pook-Kolb, B. Krishnan, and E. Schnetter, Phys. Rev. D **103**, 044054 (2021).
[43] V. Prasad, A. Gupta, S. Bose, B. Krishnan, and E. Schnetter, Phys. Rev. Lett. **125**, 121101 (2020).
[44] M. Okounkova, arXiv:2004.00671.
[45] J. L. Jaramillo and B. Krishnan, arXiv:2206.02117.
[46] Y. Chen, P. Kumar, N. Khera, N. Deppe, A. Dhani, M. Boyle, M. Giesler, L. E. Kidder, H. P. Pfeiffer, M. A. Scheel, and S. A. Teukolsky, Phys. Rev. D **106**, 124045 (2022).
[47] D. R. Brill and R. W. Lindquist, Phys. Rev. **131**, 471 (1963).
[48] J. M. Bowen and J. W. York, Phys. Rev. D **21**, 2047 (1980).
[49] For initial data corresponding to a large separation of the black holes, this parameter can be interpreted as the individual momenta of the black holes. However, these simulations have an initial separation of $0.4M_\circ$, so this interpretation is not applicable. Nonetheless, increasing P corresponds to increasing the coordinate velocities of the black holes.
[50] S. W. Hawking and J. B. Hartle, Commun. Math. Phys. **27**, 283 (1972).
[51] L. C. Stein, J. Open Source Softwaare **4**, 1683 (2019).
[52] D. Brizuela, J. M. Martin-Garcia, and G. A. Mena Marugan, Phys. Rev. D **74**, 044039 (2006).
[53] D. Brizuela, J. M. Martin-Garcia, and G. A. M. Marugan, Phys. Rev. D **76**, 024004 (2007).
[54] D. Brizuela, J. M. Martin-Garcia, and M. Tiglio, Phys. Rev. D **80**, 024021 (2009).
[55] A. Spiers, A. Pound, and B. Wardell, arXiv:2306.17847.
[56] K. Ioka and H. Nakano, Phys. Rev. D **76**, 061503(R) (2007).
[57] H. Nakano and K. Ioka, Phys. Rev. D **76**, 084007 (2007).
[58] See Supplemental Material at http://link.aps.org/supplemental/10.1103/PhysRevLett.131.231401 for full analysis of the $l = 3$, $l = 4$ and 6 shear modes. We also present the complementary analysis of the $l = 2$ shear mode for the unboosted simulation $S2$ and a detailed explanation of our numerical simulations.

[59] X. J. Forteza and P. Mourier, Phys. Rev. D **104**, 124072 (2021).
[60] We follow a similar "bootstrap" strategy as in [19], where we first confirm the presence of the fundamental tone at late times, and the first fundamental tone, before searching for higher tones.
[61] We evaluate the amplitudes on an interval of $4M$ centered around the time of the fit t_0. The range of amplitudes in the interval is the uncertainty bars in Fig. 3.
[62] A. Kehagias, D. Perrone, A. Riotto, and F. Riva, Phys. Rev. D **108**, L021501 (2023).